Biosensors and Bioelectronics xxx (2018) xxx-xxx

Contents lists available at ScienceDirect

Biosensors and Bioelectronics

journal homepage: www.elsevier.com

Chiral magnetic-nanobiofluids for rapid electrochemical screening of enantiomers at a magneto nanocomposite graphene-paste electrode

J. Muñoz[a, *], A. González-Campo[a], M. Riba-Moliner[a], M. Baeza[b], M. Mas-Torrent[a, c]

[a] Institut de Ciència de Materials de Barcelona (ICMAB-CSIC), Campus UAB, 08193 Bellaterra, Spain
[b] Departament de Química, Facultat de Ciències, Universitat Autònoma de Barcelona, Campus UAB, 08193 Bellaterra, Spain
[c] Networking Research Center on Bioengineering Biomaterials and Nanomedicine (CIBER-BBN), Campus de la UAB, 08193 Bellaterra, Spain

ARTICLE INFO

Keywords:
β-Cyclodextrin
Biosensing
Enantiorecognition
Supramolecular Chemistry
Tryptophan

ABSTRACT

The development of highly sensitive and selective enantiomeric platforms towards the rapid screening of active pharmaceutical ingredients (APIs) is nowadays a crucial challenge in several fields related to pharmacology, biomedicine, biotechnology and (bio)sensors. Herein, it is presented a novel, facile and generic methodology focused on exploiting the synergistically and electrocatalytic properties of chiral magnetic-nanobiofluids (mNBFs) with electrochemical enantiobiosensing at a magneto nanocomposite graphene paste electrode (mNC–GPE). The feasibility of this approach has been validated by chirally recognizing tryptophan (TRP) enantiomers as a proof-of-concept. For this aim, a specific chiral mNBF based on an aqueous dispersion of cobalt ferrite loaded with gold nanoparticles carrying a thiolated β-cyclodextrin (β–CD-SH/Au/$CoFe_2O_4$–NPs) has been synthesized and used towards the supramolecular discrimination of TRP enantiomers at an advanced graphene-paste transducer *via* cyclic voltammetry. This strategy, which is the first demonstration of applicability of chiral mNBFs for electrochemical enantiorecognition, opens up new approaches into enantio(bio)sensing.

1. Introduction

Chiral enantiomers have identical chemical formula, molecular weight and physicochemical properties except for optical rotation, whereas they exhibit different biological and pharmacological properties. Many biologically active substances, such as amino acids, proteins, enzymes, DNA, *etc.,* are chiral (Tiwari and Prasad, 2015). While only one enantiomer of a chiral drug, usually the L–form, exhibits useful therapeutic effects, the D–form may generate adverse reaction to living organisms. Therefore, it is crucial to develop simple, effective and generic analytical methods for chiral separation and screening of pharmaceutical intermediates and active pharmaceutical ingredients (APIs) (Ilisz et al., 2013; Meng et al., 2017). Among the twenty natural amino acids, the building blocks for proteins and important metabolites, tryptophan (TRP) is one of many important chiral compounds that play a critical role in the physiological and pharmaceutical metabolisms in biological systems (Barrett, 2012). Although only L–tryptophan (L–TRP) is desired as an API since the unbalance or deficiency of L–TRP may cause several chronic diseases, D–tryptophan (D–TRP) is an important non-protein amino acid used as intermediate to generate synthetic peptide antibiotics and immunoppressive agents in pharmaceutical industry (Dahui et al., 2002).

Various discrimination methods have been applied for enantiomeric recognition and separation of amino acids, including optical rotation (Williams, 2013), circular dichroism spectroscopy (Cao et al., 2013), high-perfomance liquid chromatography (Ilisz et al., 2006), capillary electrophoresis (Ali et al., 2014), fluorescence (Okutani et al., 2014) and electromigration techniques (Giuffrida et al., 2014), among others. Nonetheless, those approaches usually require expensive instruments and laborious sample pretreatments. Nowadays, electrochemical methods have been received considerable attention for their exploitation in this field since they are simpler, faster, cheaper and higher sensitive than the aforementioned ones (Trojanowicz, 2014; Zhu et al., 2017). However, the fabrication of efficient chiral transducer platforms for the electrochemical enanantio(bio)sensing still remain a considerable challenge. The key points to produce an electrochemical chiral sensor must be focused on two steps: *i)* engineering molecular architectures consisting of enantioselective sensing sites (recognition agents) that exhibit different binding affinity for enantiomers by forming of a supramolecu-

* Corresponding author.
Email address: jmunoz@icmab.es (J. Muñoz)

https://doi.org/10.1016/j.bios.2018.01.024
Received 21 October 2017; Received in revised form 4 January 2018; Accepted 11 January 2018
Available online xxx
0956-5663/

lar complex (Scriba, 2016) and *ii)* using materials which enhance and distinguish the analytical signal derived from the interaction on the electrode surface (optimized transducer platforms) (Muñoz et al., 2017).

Common way to achieve high sensitivity of an electrochemical sensor is to use high specific surface area electrodes made from functionalized carbon nanomaterials (Pumera, 2009). In this sense, graphene-based nanomaterials have demonstrated to exhibit a better electrochemical sensing performance than other common carbon nanoallotropes, fact that is mainly attributed to the most exposed sp^2-like planes and edge defects on the carbon sheets. Several ways for synthesizing, functionalizing or suspending graphene for further electrode modifications have been proposed (Ambrosi et al., 2014).

Cyclodextrins (CDs) are an example of recognition biomolecules that have been widely used for electrochemical approaches. CDs present a relatively low cost and an excellent capability to host effectively, selectivity and enantioselectivity various bioactive compounds into their hydrophobic cavities to form stable host-guest inclusion complexes (Zaidi, 2017; Saavedra et al., 2008; Muñoz et al., 2016b). Although modified graphene-based platforms with CDs have also been employed in few instances for the electrochemical discrimination of TRP enantiomers, such unification of enantioselectivity with electrical conductivity has been mainly based on casting graphene-based hybrid-nanomaterials containing the CD in the form of films onto pure carbon electrode surfaces (Zor et al., 2017; Xiao et al., 2017; Ou et al., 2015). This approach usually leads to a fragile modification which can result in possible diffusion problems. These drawbacks can be solved by using a nanocomposite graphene-paste electrode (NC–GPE) since the polymeric nature of the nanocomposite permits an easy and reproducible bio-functionalization (Muñoz and Baeza, 2017). Additionally, NC–GPE present different electrochemical improvements over conventional casted graphene electrodes, such as *(i)* robustness, *(ii)* renewable surface, *(iii)* small background current, *(iv)* miniaturization capability and *(v)* the possibility to behave as microelectrode array after optimizing the carbon polymer composition ratio, resulting in advanced transducers with enhanced electroanalytical performances (McCreery, 2008; Muñoz et al., 2016a; Muñoz et al., 2015). A rather recent step in the area of modification of NC-GPEs, which is derived from the malleability of the polymeric matrix, is the integration of a magnet into the carbon paste for magneto mNC–GPE development (Haghshenas et al., 2015; Muñoz and Baeza, 2017). This strategy opens up new alternatives to develop specific chiral magnetic-nanobiofluids (mNBFs) where the functionalized magnetic beads are collected after analyte interactions, pre-concentrating and stimulating the redox processes at the electrode surface as well as removing the possible matrix effect from complex samples.

Coated magnetic nanospheres consisting of a ferrite core derivate (typically cobalt ferrite nanoparticles, CF–NPs) exhibits an inverse spinel structure, high curie temperature, superior mechanical and chemical stability, large surface area and good compatibility. Among many approaches to functionalization of the surfaces of magnetic beads, one of the most promising systems involves their coating with gold nanoparticles (Au–NPs). Nanosized gold particles posses water-solubility, high chemical stability and allows fine-tuning of the surface biocompatibility (Wang et al., 2008; Kharisov et al., 2014). Thus, CF–NPs and their functionalized derivates have been exploited for their surface modification with a variety of functional (bio)molecules (*i.e.*, cellulose derivates, proteins and β–CDs), presenting interesting potential in drug delivery, catalysis, magnetic response image, bioanalysis and emphasizing its chiral recognition capability towards the discrimination of amino acids enantiomers (Guo et al., 2017; Ghosh et al., 2013; Liu et al., 2015). However, to the best of our knowledge, there has been only one recent work on their application for electrochemical chiral recognition (Shi et al., 2017).

Accordingly, the motivation for this work is derived primarily from the need of developing a rapid and simple methodology towards the electrochemical screening of enantiomeric APIs, exploiting the combined synergistically properties of chiral mNBFs and mNC–GPEs. As a first demonstration of applicability, TRP has been used as the proof chiral analyte. The present electrochemical enantiorecognition methodology, which is straightforward, generic and based on the competitive host-guest interactions (similar to antibody-antigen assay), is based on three sequential stages following Scheme 1: *A)* firstly, an aqueous dispersion based on CF–NPs decorated with Au–NPs carrying a thiolated β–CD (β–CD-SH/Au/CF–NPs) has been synthesized *via* green routes and used as the specific chiral mNBF. The strength of the gold-thiol interactions provided the basis for obtaining robust structured nanospheres that simultaneously possess chirality and magnetism properties; *B)* secondly, a mNC–GPE with an optimized composition ratio (13% w/w in carbon filler and 87% w/w in epoxy resin) has been fabricated as the highly sensitive transducer platform; and *C)* finally, a suitable amount of the chiral mNBF are captured by the mNC–GPE after TRP interacting, where TRP enantiomers are successfully electrochemically discriminated by means of cyclic voltammetry (CV).

2. Experimental

2.1. Chemicals and Reagents

Reduced Graphene Oxide (rGO) was successfully synthesized and characterized according to our previous method (Muñoz et al., 2016a). Briefly, Graphene Oxide (GO) was synthesized from flaked graphite (Sigma-Aldrich, St. Louis, MO, USA) and then reduced using ascorbic acid to obtain the conducting carbon filler material. Epotek H77A and its corresponding hardener Epotek H77B (Epoxy Technology, Billerica, MA, USA) were used as the insulating polymeric matrix. Magnetic cobalt ferrite nanoparticles (CF–NPs, 99%, particle size ~40 nm), gold dichloride hydrochloride ($HAuCl_4$, > 99.99%) and L– and D–TRP (≥ 98.0%) were purchased from Sigma-Aldrich. Neodymium magnets (diameter: 2.5 mm, height: 1.0 mm) were purchased from Supermagnete. Per-6-thio-β-cyclodextrin (β–CD-SH) was synthesized following the established methodology and used as the chiral biorecognition element (Rojas et al., 1995). All the rest of reagents were of at least analytical grade and used as received. Deionised water from a Milli-Q system (Millipore, Billerica, MA, USA) was used throughout all the experimental part.

2.2. Synthesis of the recognition platform (chiral mNBFs)

The synthetic procedure used in the current study for mNBFs development is illustrated in Scheme 1**A**. Gold decorated cobalt ferrite nanoparticles (Au/CF–NPs) were synthesized by an environmentally friendly technique. *(i)* 75 mg of CF–NPs were dispersed in 50 mL of a Milli-Q water (1.5 mg mL^{-1}) solution containing 5 drops of ethanol and ultra-sonicated for 1 h. Next, the aqueous CF–NPs suspension was added to a 250 mL round bottomed flask followed and 50 mL of 5.0 mM $HAuCl_4$ (precursor for Au–NPs synthesis) was dropped under ultrasound for 30 min. The acting force for such formation was focused on the electrostatic interactions between the hydroxyl groups contained on the CF–NPs surface and the Au^{3+} metal ion precursor (Huang et al., 2011; Junejo et al., 2013; Muñoz et al., 2016b). *(ii)* Then, the mixture was reduced with 100 mL of an aqueous 0.1 M $NaBH_4$ solution, which was added drop-wise to the reaction vessel and left to sonicate for a further 1 h, inducing the *in situ* nucleation of Au–NPs exclusively in the proximity of the CF–NPs surface. The resulting Au/CF–NPs were then removed magnetically, and washed several times with Milli-Q water and ethanol. *(iii)* The resultant product was dispersed in 100 mL of Milli-Q water (1.0 mg mL^{-1}) and ultra-sonicated for 1 h. Then, the aqueous Au/CF–NPs suspension was added to a 250 mL

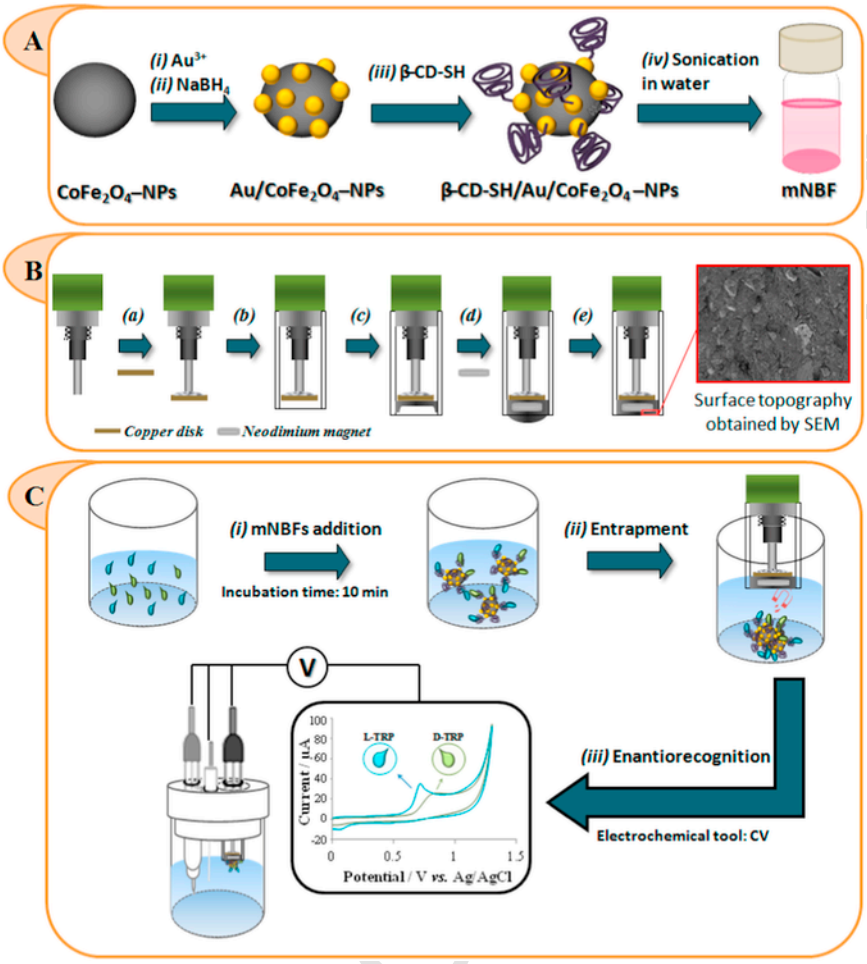

Scheme 1. Schematic illustration of A) the environmentally friendly technique carried out for chiral mNBF preparation; B) the mNC-GPE fabrication [inset: topography of the developed electrode surface based on an optimum composition of graphene/epoxy (13:87 ratio, w/w)] and C) the enantiorecognition assay for L– and D–TRP discrimination at the electrochemical cell *via* cyclic voltammetry.

round bottomed flask and set to sonicate at room temperature for 30 min. Following this, 100 mL of an aqueous (9:1 water-ethanol, v/v) 2.0 mM suspension of β–CD-SH was added and left to stir overnight. Afterwards, magnetic beads were removed magnetically and then washed several times with Milli-Q water and ethanol in order to remove the unbound β–CD-SH. *(iv)* Finally, the resulted β–CD-SH/Au/CF–NPs were re-dispersed in Milli-Q water to obtain the chiral mNBF suspension, which was stored at 4 °C for further use.

2.3. Fabrication of the transducer platform (mNC–GPEs)

A previously optimized composition of a graphene-based nanocomposite paste was hand-made prepared by mixing the conducting carbon filler (rGO) and the insulating epoxy resin in a 13:87 ratio (w/w) for 30 min (Muñoz et al., 2016a). mNC–GPEs were prepared following the methodology depicted in Scheme 1**B**. *(a)* A copper disk (5 mm of diameter and 1 mm of thickness) is soldered to a female connector (2 mm of diameter) and *(b)* introduced into a PVC tube (6 mm of internal diameter and 20 mm of length). *(c–d)* A small neodymium magnet (3 mm diameter) is placed into the center of this electrode after the addition of a thin layer of composite paste in order to avoid direct contact between the magnet and the electrical connector. *(e)* When the electrode body gap is completely filled and tightly packed, the nanocomposite-based electrode is cured at 80 °C for 24 h and finally polished with different sandpapers of decreasing grain size. Finally, the resultant mNC–GPEs, with a geometric area of 28 mm^2, were activated at +1.20 V for 1 min in a phosphate *buffered* saline (PBS) solution at pH 7.0 as a pretreatment step and used as bare electrode support for electrochemical approaches.

2.4. Tools

Physical characterization of the magnetic beads at the different functionalization stages was carried out using several techniques: Scanning Electron Microscopy (SEM) and High-Resolution Transmission Electron Microscopy (HR–TEM) images were taken using a ZEISS® MERLIN FE-SEM and a JEOL 2010-FEG unit with an acceleration voltage of 200 kV coupled to an Energy Dispersive X-Ray Spectroscopy (EDS), respectively. The magnetic behavior of the different CF-based magnetic beads was studied in a vibrating sample magnetometer (VSM) by using a Quantum Design MPMS system at room temperature with a maximum applied magnetic field of 7.5 kOe. Thermogravimetric Analysis (TGA) technique was used to quantify the total metal content in the different magnetic nanoparticles, using a Netzsch instrument; model STA 449 F1 Jupiter®. Samples were heated to 1000 °C at 10 °C/min in air flow. Electrochemical experiments were carried out by means of Electrochemical Impedance Spectroscopy (EIS) and Cyclic Voltammetry (CV), using a Novocontrol Alpha-AN impedance analyzer equipped with a potentiostat POT/GAL 30 V/2 A electrochemical interface, with a three-electrode configuration. A single junction Ag/AgCl electrode and a platinum-based electrode were used as reference and auxiliary electrodes, respectively. Bare mNC–GPEs and casted mNC–

GPEs with 200 μL of developed chiral mNBFs (for blank experiments) were used as the working electrodes. The measurements were made in a 10.0 mL of 0.1 M KCl solution containing 10 mM $K_3[Fe(CN)_6/K_4[Fe(CN)_6]]$ under quiescent condition. All the experiments were performed at room temperature and under environmental conditions. Cyclic voltammograms were carried out using a scan rate of 50 mV s^{-1}. For impedance measurements, a frequency range of 100 kHz to 0.1 Hz was employed at redox equilibrium potential (+150 mV), which was previously obtained by CV. The signal amplitude to perturb the system was 5 mV and the equilibrium time was 10 s. All the experiments were performed at room temperature and under environmental conditions. Resistance parameters were obtained by fitting the impedance spectra to the Randles equivalent circuit with Z_{view} software (Scribner Associates Inc., USA).

2.5. Enantiorecognition assay

The developed methodology is similar to a conventional antigen-antibody immunoassay, following three sequential steps (see Scheme 1**C**): *(i)* 200 μL of the synthesized chiral mNBF was incorporated into a vial containing 500 μL of a desired concentration of L–TRP, D–TRP or LD–TRP mixtures. The vial was aged for 10 min in order to promote the supramolecular interactions between β–CD and TRP enantiomers. *(ii)* The magnetic beads inside the vial were captured by dipping the activated mNC-GPE and washed twice with a PBS *buffer* solution (pH 7.0). *(iii)* Finally, loaded electrodes were transferred into the electrochemical cell filled with the PBS *buffer* solution (electrolyte) for voltammetric analysis. After each measurement, magnetic beads were removed from the mNC–GPE by a simple polishing step, obtaining a reset electrode surface. Each measurement was carried out per triplicate to determine the repeatability of the method with three different electrodes in order to estimate the reproducibility (n = 9). For blank experiments, a desired concentration of either L–TRP or D–TRP was directly added into the electrochemical cell using the bare mNC-GPE (without containing mNBFs) as the working electrode.

3. Results and discussion

3.1. Physical characterization of chiral mNBFs

The successful synthesis of the novel chiral mNBF was confirmed by High-Resolution Transmission Electron Microscopy (HR–TEM) coupled to an Energy Dispersive X-Ray Spectroscopy (EDS) and Vibrating Sample Magnetometer (VSM), as it is depicted in Fig. 1.

HR–TEM images were taken for the three different CF-based magnetic beads. Fig. 1**A** shows the commercial CF–NPs used in this study, with an average size of ~ 40–50 nm. HR–TEM micrograph in Fig. 1**B** shows a representative image of the incorporation of Au–NPs upon such magnetic beads, resulting in the Au/CF–NPs material. It is evident that CF–NPs are well decorated by a large quantity of spherical Au–NPs on their surface (with average size of 5–10 nm and rather good size distribution), and both the core CF–NPs and the Au–NPs can be clearly observed. Afterwards, the resultant hybrid-nanomaterial was used as nanotemplates for the covalently grafting of the β–CD-SH (Fig. 1**C**). The EDS spectra of the resulting β–CD-SH/Au/CF–NPs qualitatively determined the presence of Au on the core magnetic nanoparticles as well as an additional S peak provided by the incorporation of the thiolated chiral biorecognition element (see Fig. 1**D**). Additionally, a further characterization technique carried out by Fourier-Transform Infrared Spectroscopy (FTIR) also demonstrated qualitatively the Au–S bond formation, showing two additional peaks at 850 and 2300 cm^{-1} in the magnetic beads containing the biorecognition element, exclusively. Such peaks are associated to the Au–S and S–CH stretch vibration modes, respectively.

The magnetic properties of the CF-based magnetic beads at each functionalization step were measured out at room temperature by

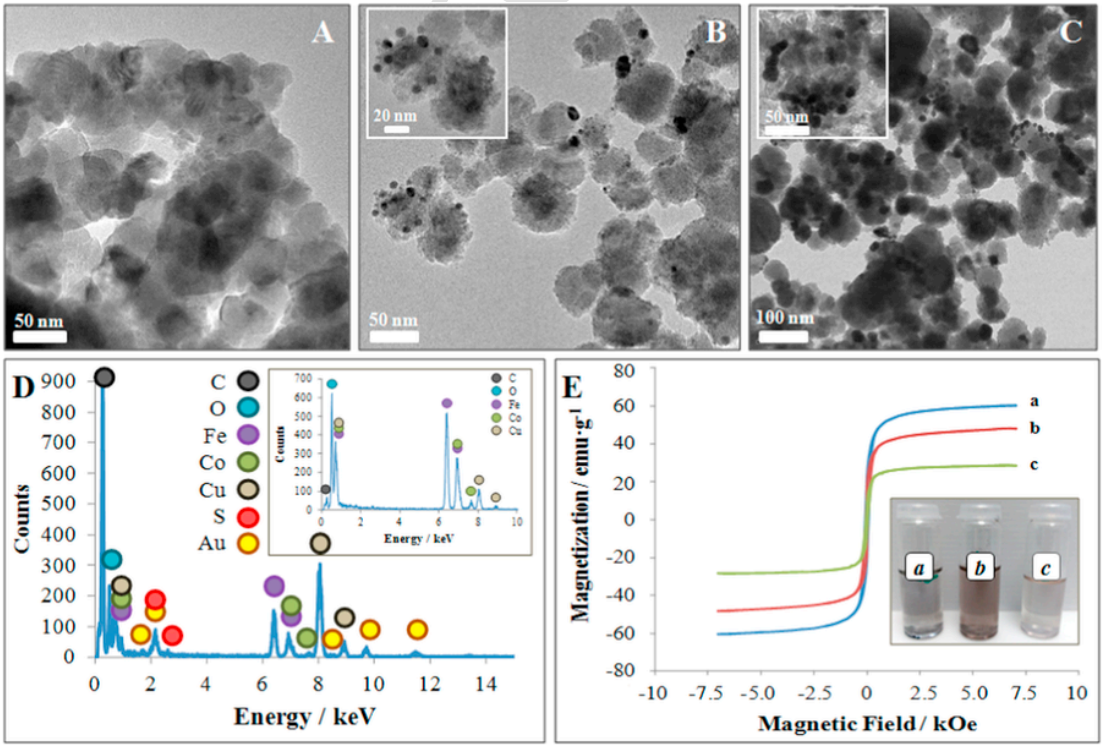

Fig. 1. HR–TEM images of A) bare CF–NPs, B) Au/CF–NPs and C) β–CD/Au/CF–NPs (inset: magnification images). D) EDS spectrum of β–CD/Au/CF–NPs (inset: EDS spectrum of bare CF–NPs for comparison). E) VSM characterization curves for *a)* bare CF–NPs, *b)* Au/CF–NPs and *c)* β–CD/Au/CF–NPs (inset: 1.0 mg mL^{-1} dispersions in water of the different magnetic beads).

VSM, as shown in Fig. 1**E**. All magnetization curves appear S-shaped over the applied magnetic field. Magnetic remanences nearly to zero were presented by the three samples, indicating that there was almost no remaining magnetization when the external magnetic field was removed, which is characteristic of a superparamagnetic behavior (Yan et al., 2009). Nonetheless, as it was expected, a significant decrease in saturation magnetization after each functionalization step was observed, decreasing from 60 emu g^{-1} for CF–NPs (*curve a*) to 48 emu g^{-1} for Au/CF–NPs (*curve b*) and 28 emu g^{-1} for β–CD-SH/Au/CF–NPs (*curve c*). This fact is explained by a decrease in the relative amount of magnetic component.(Goya et al., 2003) This is an excellent result which reflects an obvious functionalization of the magnetic beads with a high amount of both Au–NPs and β–CD-SH. A further quantitative determination of the wt% of both Au–NPs and β–CD-SH was carried out by TGA, which determined an amount of 7.8% and 6.0% in Au–NPs and β–CD-SH, respectively. These results validated again each functionalization step, pointing out the inclusion of chiral biomolecules upon the core of the functionalized magnetic beads.

A major limitation for the use of raw magnetic beads is their lack of dispersibility in aqueous media, as is shown in Fig. 1**A**. Aqueous dispersion of the different magnetic beads (1.0 mg mL^{-1}) after 30 days revealed an efficient functionalization of the material from vial *a* to vial *b* since higher dispersibility was achieved with including Au–NPs, as it was expected (see Fig. 1**E**, inset). Additionally, a much higher degree of dispersibility in water was observed after chiral biorecognition element incorporation (from vial *b* to vial *c*), highlighting the role that the β–CD play on the properties of the magnetic-nano(bio)fluids. It is worth noticing that even after three months, the chiral mNBF suspension was still stable.

3.2. Electrochemical characterization of fabricated mNC–GPEs

The benchmark $[Fe(CN)_6]^{3-/4-}$ redox marker was employed for electrochemical characterization of graphene-based transducers since it is a commonly used redox couple to investigate the electrochemical performances of modified electrode surfaces. CV provides information about the accessibility of the redox marker to be oxidized or reduced at the electrode surface by analyzing the anodic and cathodic peak currents (I_p), where the reversibility of the redox couple is defined in terms of the redox peak separation (ΔE) (Rees, 2016). Further, EIS determines the electronic transfer capabilities in the frequency domain, where the charge transfer resistance (R_{CT}) values were determined by fitting the Nyquist plots (imaginary impedance *vs.* real impedance) with a typical Randles equivalent circuit (see Fig. 2**B**, inset) (Muñoz et al., 2017).

The electrochemical behavior of bare mNC–GPE and drop-casted mNC–GPE with 200 μL of an aqueous suspension of the developed chiral mNBF (1.0 mg mL^{-1}) on the electrode surface was interrogated. Such drop-casting approach was carried out in order to reproduce the enantiorecognition assay conditions. Cyclic voltammograms from Fig. 2**A** reveals a pair of well-defined redox peaks for the bare electrode (curve *a*), with an I_p of 0.97 μA and a ΔE of 270 mV. After mNBFs casting on the electrode surface, a non-significant I_p decrease of 10% accompanied by a quite 14% increase in ΔE was observed (curve *b*), fact that might be attributed to the lower conductivity of the chiral mNBFs exposed on the electrode surface.

Further characterization experiments were carried out electrochemically by EIS technique. Fig. 2**B** shows the Nyquist plots obtained for bare and casted mNC–GPEs with chiral mNBFs (see curves *a* and *b*, respectively). The Nyquist plots of the EIS consists of two parts: a semicircular portion at higher frequencies that corresponds to the R_{CT}, an indicator reflecting the resistance at the electrode-solution interface;

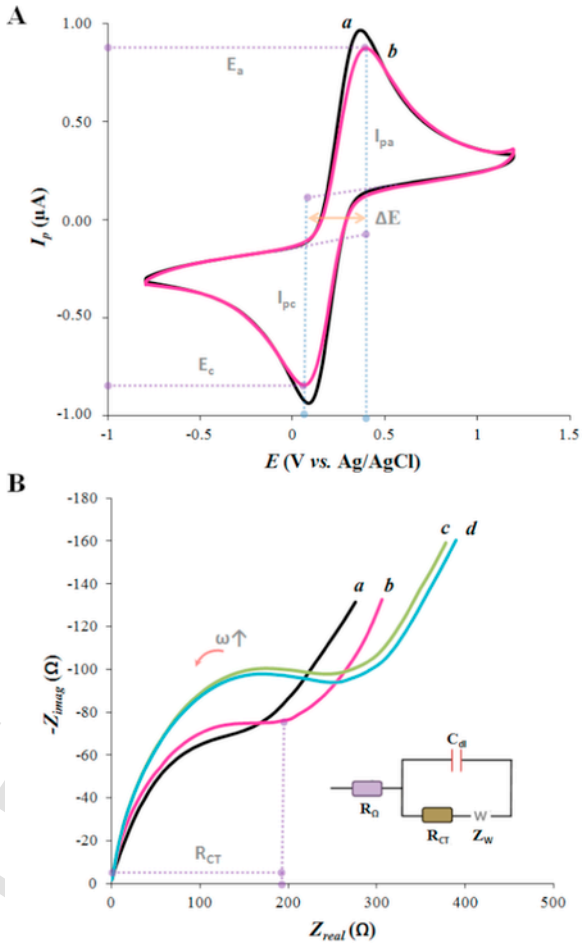

Fig. 2. A) Voltammetric characterization of *a)* bare mNC–GPE and *b)* coated mNC-GPE with chiral mNBFs (scan rate: 50 mV s^{-1}). Impedimetric characterization of *a)* bare mNC–GPE and *b)* coated mNC-GPE with chiral mNBFs before and after enantiorecognition assay with 1.0 mM of *c)* D–TRP and *d)* L–TRP (freq. range: 100 kHz–100 mHz; bias potential: +180 mV and AC amplitude: 5 mV; inset: Randles equivalent circuit). Electrochemical experiments were carried out using a 0.1 M KCl aqueous solution containing 10 mM $[Fe(CN)_6]^{3-/4-}$ as the benchmark redox marker.

and a linear portion at lower frequencies which is related to the diffusion limited process.

As it was expected from CV experiments, a significant R_{CT} increase from 173.8 Ω to 205.7 Ω was observed after electrode surface modification with the chiral mNBFs owing to the lower conductivity of magnetic beads containing the β–CD. Casted mNC–GPEs with chiral mNBFs were also evaluated following the enantiorecognition assay methodology after incubating them in an aqueous solution containing 1.0 mM of either D–TRP or L–TRP for 10 min (see curves *c* and *d*, respectively). This procedure was carried out in order to verify the supramolecular recognition properties of β–CD towards TRP enantiomers. In both cases, a significant increase on the R_{CT} parameter from 205.7 Ω to 270.9 Ω for D–TRP and 272.4 Ω for L–TRP was obtained due to the formation of an insulating supramolecular complex on the electrode surface that hinders the interfacial electron transfer kinetics between the redox probe and the electrode. Nonetheless, no significant differences by means of R_{CT} (< 1%) were observed between TRP enantiomers, not being possible to identify them. These results indicate that EIS technique is not a suitable electrochemical tool to discriminate between TRP enantiomers since non interfacial resistance difference between them was achieved.

3.3. Electrochemical chiral recognition of TRP enantiomers

The electrochemical responses of 1.0 mM of the enantiomeric pairs combined with the mNBFs were recorded at the prepared mNC–GPEs by CV, following the aforementioned enantiorecognition assay. Initially, control experiments were carried out at the bare mNC–GPE (without chiral mNBFs) by adding the same concentration of separately TRP enantiomers directly into the electrochemical cell. As it is shown in Fig. 3**A**, no enantiomeric resolution was achieved at the bare mNC–GPE since the two oxidation peaks are completely overlapped. Accordingly, L–TRP and D–TRP cannot be discriminated at the bare mNC–GPE. However, when chiral mNBFs were captured by the mNC–GPE after the enantiorecogntion assay for the two separated enantiomers (Fig. 3**B**), high distinguishable differences in both I_p and peak-to-peak separation (ΔE_{L-D}) were observed due to the inclusion complex generation between TRP enantiomers and β–CD. A recognition efficiency estimated by means of peak current ratio (I_L/I_D) of 1.40 and ΔE_{L-D} of 140 mV was achieved, pointing out that the chiral mNBFs preferentially recognize L–TRP over D–TRP. Compared to the bare mNC–GPE, both I_L and I_D currents increased after the enantiorecogntion assay from 16.9 μA (see Fig. 3**A**) to 32.2 μA and 25.6 μA (see Fig. 3**B**) for L–TRP and D–TRP, respectively. These results demonstrate that the chiral mNBFs also act as electrocatalytic mediator toward the oxidation of

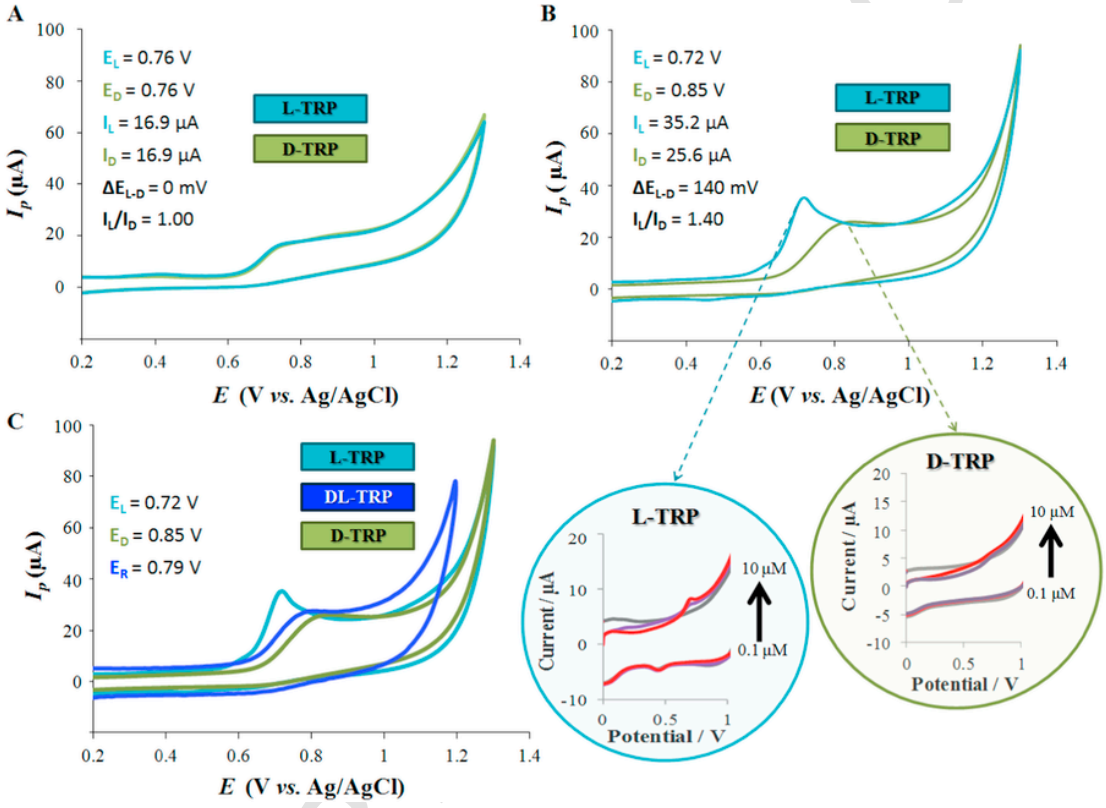

Fig. 3. Cyclic voltammograms in the absence and presence of 1.0 mM D–TRP and L–TRP at A) bare mNC–GPE and B) chiral recognition platform; inset: voltammetric response upon increasing concentrations of L–TRP and D–TRP in a low concentration range (0.1 μM and 10 μM). C) Enantiomeric mixtures of TRP at different ratios of D–TRP and L–TRP (1:0, 1:1 and 0:1, c/c). Electrochemical experiments were carried out in a PBS *buffer* solution (pH 7.0). Scan rate: 25 mV s^{-1}.

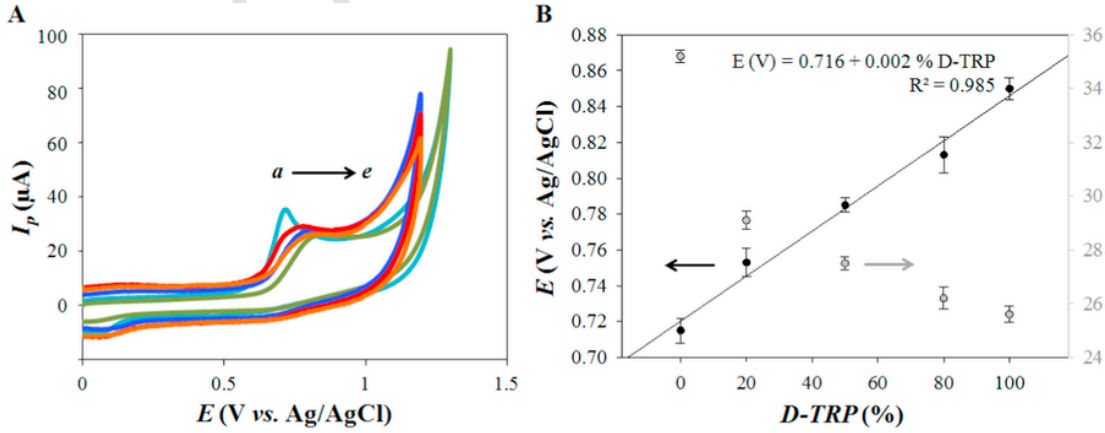

Fig. 4. Enantiomeric mixtures of TRP represented as D–TRP (%) for *a)* 0% *b)* 20% *c)* 50% *d)* 80% and *e)* 100%. A) Cyclic voltammograms and B) calibration curves depicting the redox potential (black plots) and current intensity peaks (grey plots) *vs.* the percentage of D–TRP. Electrochemical experiments were carried out in a PBS *buffer* solution (pH 7.0). Scan rate: 25 mV s^{-1}.

TRP, fact that can be ascribed to the pre-concentration stage realized *via* magnetic field-induction on the electrode surface.

Importantly, the oxidation peak sharpness varies between TRP enantiomers, showing a sharper and narrower peak for L–TRP than D–TRP. The current peaks width mainly depends on the diffusion-process contribution, which is more significant for broader peaks (Costentin et al., 2012). Such differences in enantioselectivity can be attributed to different kinetics and thermodynamics phenomena. A key parameter is the shape selectivity of the β–CD cavity accompanied by the divergent inclusion binding strength between guests (TRP enantiomers) and host (β–CD). Thus, the larger and sharper I_p obtained from L–TRP are in agreement with the stability constant (log *K*) of the inclusion complex reported in literature for L–TRP and D–TRP with β–CD, which should be 2.33 and 1.11, respectively (Rekharsky and Inoue, 1998). This is mainly attributed to a more preferable inclusion of L–TRP on the β–CD cavity rather than D–TRP because of the favorability of H-bond formation between the secondary hydroxyl groups on β–CD rims and the amino group of L–TRP when the indole group of TRP isomers inserts into its cavity (Tao et al., 2014).

Additionally, further voltammetric experiments were tested at the electrochemical recognition platform using lower concentrations of TRP enantiomers (0.1 and 10 μM), as shown in Fig. 3**B** (oval insets). While no response for the D–TRP was exhibited by redox peaks means, the electrochemical recognition system was capable to determine L–TRP at such low concentrations, opening up a working range of enantiomeric discrimination. These results highlight again the preference of the functionalized-mNBFs with β–CD towards L–TRP, phenomena that must be ascribed to electrocatalytic and kinetic (*K*) factors.

3.4. Electrochemical determination of TRP enantiomers

Voltammograms for enantiomeric mixtures of TRP at different ratios of L–TRP and D–TRP (1:0, 1:1 and 0:1, c/c) with a total concentration of 1.0 mM determined an excellent correlation with a racemic redox potential (E_R) of: $E_R = \frac{E_L+E_D}{2} = 0.79$ V; which in fact corresponds to the redox potential value expected for a racemic mixture (see Fig. 3**C**). These results verified the capability of the developed enantiorecognition platform towards the discrimination of racemates. Such promising results demonstrated that the functionalized-mNBFs can provide a chiral microenvironment at the mNC–GPE for enantioselective combination *via* supramolecular chemistry with TRP enantiomers.

Additionally, Fig. 4**A** shows how it was possible to evaluate the enantiomeric excess with other enantiomeric percentage of L–TRP and D–TRP, where only one broad oxidation peak was found regardless of the relative content of D–TRP (%) in the enantiomeric mixtures. As it is presented in Fig. 4**B**, while peak potential shifted lineally to the right (anodically) with good correlation curve ($R^2 = 0.985$), peak current significantly decreased with increasing the percentage of D–TRP.

Interestingly, it is very important to note how the shape of the oxidation peaks changes drastically when the solution contains some percentage of D–TRP, being able to discriminate easily whether the solution is pure in L–TRP or if it contains some D–TRP impurities. Since the L–TRP is the desired API enantiomer, the proposed chiral recognition method could be firmly exploited for the rapid screening of TRP enantiomers.

In concordance with a very recent report, it is also important to highlight that the influence of some typical electroactive biomolecules, such as glucose, fructose, maltose, glycine, alanine, proline and tyrosine, among others, as well as common ions (*i.e.*, Ca^{2+}, Fe^{2+}, Fe^{3+}, NO_3^-) do not present significant interferences on the electroanalytical response of TRP enantiomers at a graphene-based sensor containing β–CD as the biorecognition element, even in the presence of higher concentration of these substances [Xiao et al. (2017)]. Thus, the present chiral mNBFs, in combination with the highly sensitive graphene-based electrode platform (mNC–GPE) clearly show their potential for the analysis in real samples, which will be subject of study in the near future.

4. Conclusions

It has been successfully developed a novel, fast and generic magneto enantiorecognition methodology for electrochemical discrimination purposes through the synergistic and electrocatalytic combination of chiral mNBFs and mNC–GPEs. As a proof-of-concept, TRP enantiomers have been electrochemically discriminated at an optimized mNC–GPE, using graphene as highly sensitive conducting nanostructured carbon filler. For this aim, specific chiral mNBFs based on the covalently grafting of a thiolated β–CD on Au–NPs deposited on cobalt ferrite magnetic beads were synthesized *via* green routes. Importantly, such chiral mNBFs exhibit outstanding dispersibility and stability in water. The present electrochemical methodology not only discriminates between L–TRP and D–TRP enantiomers but also between enantiomers concentrations and racemic mixtures. Further, it has been demonstrated that by analyzing the changes observed in the oxidation peak shapes, this electrochemical recognition platform can be exploited as a rapid screening system of the pure API compound among contaminated mixtures with D–TRP. Finally, this approach might be easily customized and extended towards the enantio(bio)sensing of alternative APIs through the development of novel mNBFs carrying specific chiral selectors, which is a crucial challenge in pharmacological and biotechnological phenomena.

Acknowledgments

This work was funded by the ERC StG 2012–306826 e-GAMES. The authors also thank the Networking Research Center on Bioengineering, Biomaterials, and Nanomedicine (CIBER-BBN), the DGI (Spain) project FANCY CTQ2016-80030-R, the Generalitat de Catalunya (2014-SGR-17), the MAT2016-77852-C2-1-R (AEI/FEDER, UE) and the Spanish Ministry of Economy and Competitiveness, through the "Severo Ochoa" Programme for Centers of Excellence in R&D (SEV-2015-0496).

References

Ali, I., Al-Othman, Z.A., Al-Warthan, A., Asnin, L., Chudinov, A., 2014. Advances in chiral separations of small peptides by capillary electrophoresis and chromatography. J. Sep. Sci. 37 (18), 2447–2466.

Ambrosi, A., Chua, C.K., Bonanni, A., Pumera, M., 2014. Electrochemistry of graphene and related materials. Chem. Rev. 114 (14), 7150–7188.

Barrett, G., 2012. Chemistry and Biochemistry of the Amino Acids. Springer Science & Business Media.

Cao, H., Zhu, X., Liu, M., 2013. Self-assembly of racemic alanine derivatives: unexpected chiral twist and enhanced capacity for the discrimination of chiral species. Angew. Chem. Int. Ed. 52 (15), 4122–4126.

Costentin, C., Drouet, S., Robert, M., Savéant, J.-M., 2012. Turnover numbers, turnover frequencies, and overpotential in molecular catalysis of electrochemical reactions. cyclic voltammetry and preparative-scale electrolysis. J. Am. Chem. Soc. 134 (27), 11235–11242.

Dahui, W., Ping, W., Pingkai, O., 2002. Advance in studying on D-tryptophan. Chem. Ind. Eng. Progress. 21 (2), 103–105.

Ghosh, S., Fang, T.H., Uddin, M., Hidajat, K., 2013. Enantioselective separation of chiral aromatic amino acids with surface functionalized magnetic nanoparticles. Colloids Surf. B: Biointerfaces 105, 267–277.

Giuffrida, A., Maccarrone, G., Cucinotta, V., Orlandini, S., Contino, A., 2014. Recent advances in chiral separation of amino acids using capillary electromigration techniques. J. Chromatogr. A 1363, 41–50.

Goya, G., Berquo, T., Fonseca, F., Morales, M., 2003. Static and dynamic magnetic properties of spherical magnetite nanoparticles. J. Appl. Phys. 94 (5), 3520–3528.

Guo, L.-D., Song, Y.-Y., Yu, H.-R., Pan, L.-T., Cheng, C.-J., 2017. Novel smart chiral magnetic microspheres for enantioselective adsorption of tryptophan enantiomers. Appl. Surf. Sci. 407, 82–92.

Haghshenas, E., Madrakian, T., Afkhami, A., 2015. A novel electrochemical sensor based on magneto Au nanoparticles/carbon paste electrode for voltammetric determination of acetaminophen in real samples. Mater. Sci. Eng.: C 57, 205–214.

Huang, P., Li, Z., Lin, J., Yang, D., Gao, G., Xu, C., Bao, L., Zhang, C., Wang, K., Song, H., 2011. Photosensitizer-conjugated magnetic nanoparticles for in vivo simultaneous

magnetofluorescent imaging and targeting therapy. Biomaterials 32 (13), 3447–3458.
Ilisz I. Berkecz R. Péter A. 2006. HPLC separation of amino acid enantiomers and small peptides on macrocyclic antibiotic-based chiral stationary phases: a review J. Sep. Sci. 29 (10), 1305–1321
Ilisz, I., Aranyi, A., Péter, A., 2013. Chiral derivatizations applied for the separation of unusual amino acid enantiomers by liquid chromatography and related techniques. J. Chromatogr. A 1296, 119–139.
Junejo, Y., Baykal, A., Sözeri, H., 2013. Simple hydrothermal synthesis of Fe3O4-PEG nanocomposite. Open Chem. 1527.
Kharisov, B.I., Dias, H.R., Kharissova, O.V., Vázquez, A., Pena, Y., Gomez, I., 2014. Solubilization, dispersion and stabilization of magnetic nanoparticles in water and non-aqueous solvents: recent trends. RSC Adv. 4 (85), 45354–45381.
Liu, Y., Tian, A., Wang, X., Qi, J., Wang, F., Ma, Y., Ito, Y., Wei, Y., 2015. Fabrication of chiral amino acid ionic liquid modified magnetic multifunctional nanospheres for centrifugal chiral chromatography separation of racemates. J. Chromatogr. A 1400, 40–46.
McCreery, R.L., 2008. Advanced carbon electrode materials for molecular electrochemistry. Chem. Rev. 108 (7), 2646–2687.
Meng, C., Sheng, Y., Chen, Q., Tan, H., Liu, H., 2017. Exceptional chiral separation of amino acid modified graphene oxide membranes with high-flux. J. Membr. Sci. 526, 25–31.
Muñoz, J., Baeza, M., 2017. Customized bio-functionalization of nanocomposite carbon paste electrodes for electrochemical sensing: a mini review. Electroanalysis
Muñoz, J., Cespedes, F., Baeza, M., 2015. Effect of carbon nanotubes purification on electroanalytical response of near-percolation amperometric nanocomposite sensors. J. Electrochem. Soc. 162 (8), B217–B224.
Muñoz, J., Brennan, L.J., Céspedes F. Gun'ko Y.K. Baeza, M., 2016. Characterization protocol to improve the electroanalytical response of graphene–polymer nanocomposite sensors. Compos. Sci. Technol. 125 71–79.
Muñoz, J., Riba-Moliner, M., Brennan, L.J., Gun'ko, Y.K., Céspedes, F., González-Campo, A., Baeza, M., 2016. Amperometric thyroxine sensor using a nanocomposite based on graphene modified with gold nanoparticles carrying a thiolated β-cyclodextrin. Microchim. Acta 183 (5), 1579–1589.
Muñoz J. Montes R. Baeza M. 2017. Trends in electrochemical impedance spectroscopy involving nanocomposite transducers: characterization, architecture surface and bio-sensing TrAC Trends Anal. Chem.
Okutani, K., Nozaki, K., Iwamura, M., 2014. Specific chiral sensing of amino acids using induced circularly polarized luminescence of bis (diimine) dicarboxylic acid europium (III) complexes. Inorg. Chem. 53 (11), 5527–5537.
Ou, J., Zhu, Y., Kong, Y., Ma, J., 2015. Graphene quantum dots/β-cyclodextrin nanocomposites: a novel electrochemical chiral interface for tryptophan isomer recognition. Electrochem. Commun. 60, 60–63.
Pumera, M., 2009. Electrochemistry of graphene: new horizons for sensing and energy storage. Chem. Rec. 9 (4), 211–223.
Rees, N.V., 2016. Electrochemistry Fundamentals: Nanomaterials Evaluation and Fuel Cells. Nanomaterials for Fuel Cell Catalysis. Springer, 1–29.
Rekharsky, M.V., Inoue, Y., 1998. Complexation thermodynamics of cyclodextrins. Chem. Rev. 98 (5), 1875–1918.
Rojas, M.T., Koeniger, R., Stoddart, J.F., Kaifer, A.E., 1995. Supported monolayers containing preformed binding sites. Synthesis and interfacial binding properties of a thiolated. beta.-cyclodextrin derivative. J. Am. Chem. Soc. 117 (1), 336–343.
Saavedra, L., Nickerson, B., Borjas, R.E., Lynen, F., Sandra, P., 2008. Enantioseparation of pharmaceutical compounds by multiplexed capillary electrophoresis using highly sulphated α-, β-and γ-cyclodextrins. J. Chromatogr. B 875 (1), 248–253.
Scriba, G.K., 2016. Chiral recognition in separation science–an update. J. Chromatogr. A 1467, 56–78.
Shi, X., Wang, Y., Peng, C., Zhang, Z., Chen, J., Zhou, X., Jiang, H., 2017. Enantiorecognition of tyrosine based on a novel magnetic electrochemical chiral sensor. Electrochim. Acta 241, 386–394.
Tao, Y., Dai, J., Kong, Y., Sha, Y., 2014. Temperature-sensitive electrochemical recognition of tryptophan enantiomers based on β-cyclodextrin self-assembled on poly (L-glutamic acid). Anal. Chem. 86 (5), 2633–2639.
Tiwari, M.P., Prasad, A., 2015. Molecularly imprinted polymer based enantioselective sensing devices: a review. Anal. Chim. Acta 853, 1–18.
Trojanowicz, M., 2014. Enantioselective electrochemical sensors and biosensors: a mini-review. Electrochem. Commun. 38, 47–52.
Wang, L., Park, H.-Y., Stephanie, I., Lim, I., Schadt, M.J., Mott, D., Luo, J., Wang, X., Zhong, C.-J., 2008. Core@ shell nanomaterials: gold-coated magnetic oxide nanoparticles. J. Mater. Chem. 18 (23), 2629–2635.
Williams, R.M., 2013. Synthesis of Optically Active Alpha-amino Acids. Elsevier.
Xiao, Q., Lu, S., Huang, C., Su, W., Zhou, S., Sheng, J., Huang, S., 2017. An electrochemical chiral sensor based on amino-functionalized graphene quantum dots/β-cyclodextrin modified glassy carbon electrode for enantioselective detection of tryptophan isomers. J. Iran. Chem. Soc. 1–14.
Yan, H., Zhang, J., You, C., Song, Z., Yu, B., Shen, Y., 2009. Influences of different synthesis conditions on properties of Fe 3 O 4 nanoparticles. Mater. Chem. Phys. 113 (1), 46–52.
Zaidi, S.A., 2017. Facile and efficient electrochemical enantiomer recognition of phenylalanine using β-cyclodextrin immobilized on reduced graphene oxide. Biosens. Bioelectron. 94, 714–718.
Zhu, H., Chang, F., Zhu, Z., 2017. The fabrication of carbon nanotubes array-based electrochemical chiral sensor by electrosynthesis. Talanta 166 (Supplement C), 70–74.
Zor, E., Morales-Narváez, E., Alpaydin, S., Bingol, H., Ersoz, M., Merkoçi, A., 2017. Graphene-based hybrid for enantioselective sensing applications. Biosens. Bioelectron. 87, 410–416.